

Fractal ion-channel behavior generates fractal firing patterns in neuronal models

Steven B. Lowen

Department of Electrical and Computer Engineering, 8 Saint Marys Street, Boston University, Boston, Massachusetts 02215

Larry S. Liebovitch

Center for Complex Systems, Center for Molecular Biology and Biotechnology, and Department of Psychology, Florida Atlantic University, Boca Raton, Florida 33431

John A. White

Department of Biomedical Engineering, Boston University, Boston, Massachusetts 02215

(Received 10 December 1998)

Fractal behavior has been observed in both ion-channel gating and neuronal spiking patterns, but a causal relationship between the two has not yet been established. Here, we examine the effects of fractal ion-channel activity in modifications of two classical neuronal models: Fitzhugh-Nagumo (FHN) and Hodgkin-Huxley (HH). For the modified FHN model, the recovery variable was represented as a population of ion channels with either fractal or Markov gating characteristics. Fractal gating characteristics changed the form of the interspike interval histogram (ISIH) and also induced fractal behavior in the firing rate. For the HH model, the K^+ conductance was represented as a collection of ion channels with either quasifractal or Markov gating properties. Fractal gating induced fractal-rate behavior without changing the ISIH. We conclude that fractal ion-channel gating activity is sufficient to account for fractal-rate firing behavior. [S1063-651X(99)11205-4]

PACS number(s): 87.17.Nn, 87.16.Uv, 87.17.Aa, 02.50.Ey

I. INTRODUCTION

A pervasive and important problem in neuroscience is to understand how the structure and function at one level of organization is manifest in the structure and function at higher and larger levels of organization. For example, at the molecular level, the voltage and current across the cell membrane is controlled by ion channel proteins. At a higher level of organization, information of relevance is represented in the rate or timing of action potentials. In this paper, we use numerical simulations to explore the influence of the kinetics of ion channels on the statistical properties of the durations of times between action potentials. We show that different models of ion channel kinetics produce fundamentally different interspike interval statistics.

In classical models of voltage-gated conductances and underlying ion channels [1–3], it is assumed that the ion channels switch between a small number of states with kinetic rate constants that depend only on the present state of the channel. In this Markov process formulation, the time the channel has already spent in that state and the history of the previous states of the channel are irrelevant. The physical interpretation of this model is that the physical state of the ion channel at one time does not depend on its physical state at an earlier time.

That such a complex protein, consisting of thousands of amino acids that are acted upon by an array of forces (e.g., random thermal forces, atomic bonds, and electrostatic and hydrophobic forces), should exhibit memoryless behavior is counterintuitive, and in fact a large body of experimental [4–10] and computational [11,12] evidence indicates that at least some ion channels and other proteins exhibit significant memory effects [13]. In the case of ion channels, this

memory can take the form of kinetic rate constants that are not constant but rather are *fractal* [14,15], in that the rate constants are proportional to t^{-c} , where t is the time the channel had already spent in a given state and c is a constant [15–18].

At the systems level, analysis of spike trains from a variety of neuronal preparations [19–25] has shown several hallmarks of fractal behavior in interspike interval statistics. These effects include a slow decrease of fluctuations of firing rate about the mean as the rate is computed over longer time periods; a periodogram that decreases in a power-law fashion with frequency; and an Allan factor that increases as a power-law function of the counting time [26]. We illustrate this behavior by including results recorded from a representative auditory-nerve fiber in cat, stimulated by a pure tone at the characteristic (most sensitive) frequency, which was 10.2 kHz for this particular neuron [27]. Statistics obtained from this recording are included in the plots of Fitzhugh-Nagumo and Hodgkin-Huxley simulation results that follow.

What is the origin of the fractal characteristics found in the timing of action potentials recorded from nerves? While a number of different causes have been proposed [28,29], fractal fluctuations in the membrane voltage [30,31] appear to provide the best explanation. It seems reasonable to ask if the fractal kinetics of the ion channels are responsible for the fractal fluctuations in the membrane voltage, and therefore for the fractal characteristics of the action potential timing. In this paper we determine how the kinetics of ion channels influence the timing of the action potentials in the classic Fitzhugh-Nagumo and Hodgkin-Huxley neuronal models. We find that Markov and fractal ion channel kinetics produce different statistical properties in the timing of the action potentials. Our results suggest that the fractal properties found

for the timing of the action potentials may arise from the fractal kinetics of ion channels.

II. METHODS

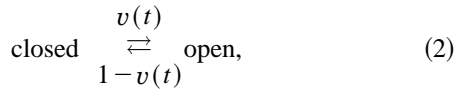
A. Markov Fitzhugh-Nagumo simulation

The Fitzhugh-Nagumo equations provide a symbolic model of neuronal activity, in which all dynamical variables of the neuron are reduced to two quantities: the ‘‘voltage’’ variable $v(t)$, which corresponds to the membrane voltage, and the ‘‘recovery’’ variable $w(t)$, which corresponds to refractory properties of the neuron. The equations are

$$\begin{aligned} \tau dv(t)/dt &= v(t)[v(t) - a][1 - v(t)] + s(t) - w(t), \\ dw(t)/dt &= v(t) - w(t), \end{aligned} \quad (1)$$

where τ and a are parameters of the system, and $s(t)$ is an input signal. For these simulations, we choose $\tau = 0.005$ to keep the time scales of $v(t)$ and $w(t)$ well separated, and $s(t) = a = 1/2$ (a constant) for simplicity. None of these choices qualitatively affects the results we present for this or the fractal Fitzhugh-Nagumo simulations, nor does the choice of v_Δ below.

To explore the effects of finite-size ion channels on the Fitzhugh-Nagumo model, we recast $w(t)$ as the proportion of channels that are open. For a finite number of channels N , then $W(t) \equiv Nw(t)$ will be open, and $N - W(t)$ will be closed. This permits the representation of Eq. (1b) by a two-state Markov process



where $v(t)$ and $1 - v(t)$ become the opening and closing rates, respectively, since

$$\begin{aligned} dw(t)/dt &= \frac{dW(t)/dt}{N} = \frac{v(t)[N - W(t)] - [1 - v(t)]W(t)}{N} \\ &= v(t) - w(t) \end{aligned} \quad (3)$$

as defined in Eq. (1b). Since each channel is interchangeable with the next, and represented by a memoryless process, we need only keep track of the *number* of channels in the two states, greatly facilitating the simulation. To ensure that the transition rates $v(t)$ and $1 - v(t)$ are non-negative, we restrict $v(t)$ to lie in the range $0 \leq v(t) \leq 1$.

The simulation is updated as follows. At each iteration an exponentially distributed random variable t_s with a mean depending on $W(t)$ and $v(t)$ is generated, which represents the time to the next channel transition. The rate of change $dv(t)/dt$ derives from Eq. (1a); over the time t_s the resulting increment of $v(t)$ would be $t_s dv(t)/dt$. If this increment exceeds a threshold v_Δ ($= 0.02$), then the voltage is incremented by v_Δ , and the time incremented by $v_\Delta / [dv(t)/dt]$; no channel states change. Otherwise, the voltage is incremented by $t_s dv(t)/dt$, and a random channel state is changed [with the probabilities of the two possible transitions also depending appropriately on $W(t)$ and $v(t)$]. The cycle then repeats. We define the Fitzhugh-Nagumo model to

have fired each time $v(t)$ first exceeds 0.8, following at least one occurrence of $v(t) < 0.2$ since the last firing. One hundred simulations were run for 2.2×10^5 seconds each, with different random seeds. The results were quite similar among the trials; results from two representative simulations are shown in the following.

B. Fractal Fitzhugh-Nagumo simulation

For the Markov ion channels employed in the above simulation, the channel behavior is memoryless, and therefore does not depend on past activity. This permits the use of a single number, $W(t)$, to describe the states of all the channels. Markov behavior also implies exponentially distributed times between switching events (given a fixed voltage).

Ion channels with fractal behavior, in contrast, have memory. Thus the time each channel has spent in its present state influences its behavior, and the probability density function $p(\tau)$ of the times between switching events no longer follows an exponential form. Rather, the interevent times often decay as a power-law function [15–17, 26, 19–21, 28, 29, 22–25, 32, 18]. For analytical convenience [33], we choose the functional form

$$p(\tau) = a \tau_0^a (\tau + \tau_0)^{-(a+1)} \quad (4)$$

over non-negative τ , with τ_0 and a positive parameters; without loss of generality we set $\tau_0 = 1$. Similar power-law forms for $p(\tau)$ yield qualitatively similar results. Setting the mean dwell times in the two states for this probability density function equal to those for the Markov case yields

$$a = \begin{cases} 1 + v & \text{for opening} \\ 2 - v & \text{for closing.} \end{cases} \quad (5)$$

Simulation becomes much more complicated (and computationally intensive) than for the Markov case, since for each channel the remaining times to the next switching event must be updated every time the voltage changes. Ten simulations were run for 10^8 seconds each, using different random seeds. The results were qualitatively similar among the trials; results from two representative simulations are shown in the following. Fractal channels have memory and hence respond more slowly than Markov channels. This greatly reduces the overall firing rate, requiring a much longer simulation time for the same number of spikes.

C. Markov Hodgkin-Huxley simulation

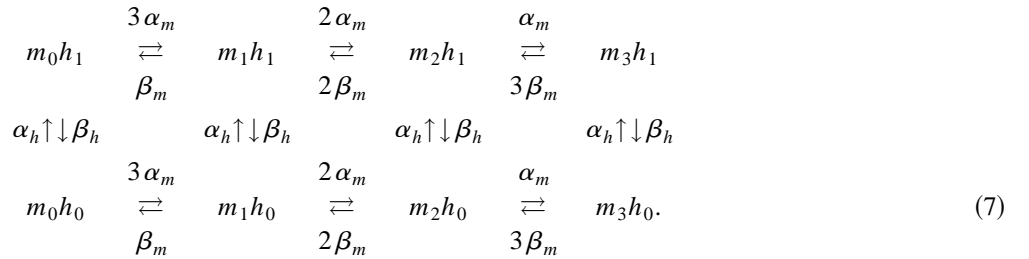
The Hodgkin-Huxley equations describe neuronal activity phenomenologically as the product of a set of nonlinear conductances. The classical equations for an isopotential patch of membrane are

$$\begin{aligned} C dv/dt &= -[\bar{g}_{\text{Na}} m^3 h (v - v_{\text{Na}}) \\ &\quad + \bar{g}_{\text{K}} n^4 (v - v_{\text{K}}) + g_L (v - v_L) - I], \\ dm/dt &= \alpha_m (1 - m) - \beta_m m, \\ dh/dt &= \alpha_h (1 - h) - \beta_h h, \\ dn/dt &= \alpha_n (1 - n) - \beta_n n, \end{aligned} \quad (6)$$

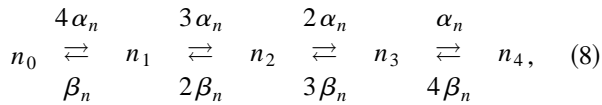
where C is membrane capacitance per unit area; v is membrane potential; \bar{g}_{Na} and \bar{g}_{K} are maximal values of the sodium- and potassium-sensitive conductances per unit area, respectively; m , h , and n are the sodium-conductance activation function, sodium-conductance inactivation function, and potassium-conductance activation functions, respectively; v_{Na} , v_{K} , and v_L are the reversal potentials associated with sodium, potassium, and leakage conductances, respectively; g_L is the Ohmic leakage conductance per unit area; and I represents current density from an external source (e.g., an intracellular electrode). While the Hodgkin-Huxley equations are less compact than the Fitzhugh-Nagumo equations, conductance-based equations have the great advantage that the variables in question can be measured experimentally under a voltage clamp. In this work, we used the classical values of Hodgkin-Huxley parameters at 6 °C [1,34], translated into the modern voltage convention.

Our method differs from that of Ref. [1] in two important

respects, however. Their equations treated the membrane variables as *continuous* and *deterministic*; the variables can take any of an infinite number of possible values along a continuum, and display no randomness whatsoever. In our models, we follow the behavior of individual channels, which are *discrete* and *stochastic*; each channel can take only one of two possible values, and the channels change state in a random manner. The conductances in the channel-based Hodgkin-Huxley models we employ are thus produced by the summed actions of voltage-gated and ion-selective channels, each of which is a stochastic device. The voltage- and time-dependent sodium conductance ($\bar{g}_{\text{Na}}m^3h$) can be represented as the product of the conductance of a single open Na^+ channel (γ_{Na}) and the number of open Na^+ channels per unit area. In our channel-based description of the Hodgkin-Huxley equation, Each Na^+ channel is a Markov process with the following rate scheme [2]:



In this scheme only the state m_3h_1 is open. Similarly, the potassium conductance ($\bar{g}_{\text{K}}n^4$) is the product of γ_{K} and the mean number of open K^+ channels per unit area. Potassium channels have the rate scheme [2]



where the lone open state is state n_4 . For this rate scheme, standard Markov analysis yields the average open and closed times for the K^+ channels:

$$\begin{aligned}
 E[T_O] &= 1/(4\beta_n), \\
 E[T_C] &= \frac{(\alpha_n + \beta_n)^4 - \alpha_n^4}{4\alpha_n^4\beta_n}.
 \end{aligned} \quad (9)$$

In our stochastic Hodgkin-Huxley algorithm, which has been described in detail previously [35,36,34], we take advantage of the memoryless property of Markov processes by tracking only the number of Na^+ and K^+ channels in each possible state. We establish an initial distribution of states

from the expected values at rest. We update this distribution by drawing the time of next state transition from a joint probability density function, and determine the specific transition that occurred from a conditional distribution [34]. We then update the value of V by integrating the current-balance equation and begin the process anew. In this work, we assume $\gamma_{\text{Na}} = \gamma_{\text{K}} = 20$ pS and channel densities of 60 (Na^+) and 18 (K^+) channels/ μm^2 , giving the same maximal conductances as in the deterministic model [34]. We model a membrane patch of area 10 μm^2 . The number of channels in the modeled patch (600 Na^+ channels, 180 K^+ channels) is small enough for channel noise to generate spontaneous activity [36,34]. We report detailed statistics on two runs: one with zero current input, and one with -4 $\mu\text{A}/\text{cm}^2$, yielding different average interspike intervals, as expected. Simulations were run for 117 027 and 87 905 spike events, respectively.

D. Fractal Hodgkin-Huxley simulation

As in the case for the Fitzhugh-Nagumo model, fractal behavior was imparted to the ‘‘recovery’’ variable, in this case the K^+ conductance. To this end, we replaced the five-state nonfractal model shown in Eq. (8) with an eleven-state rate scheme of the form

$$\begin{array}{ccccccccc}
\alpha_n^*/k^9 & & \alpha_n^*/k^8 & & \alpha_n^*/k^7 & & \alpha_n^*/k & & \alpha_n^* \\
n_0^* \rightleftharpoons & n_1^* & \rightleftharpoons & n_2^* & \rightleftharpoons & \cdots & \rightleftharpoons & n_9^* & \rightleftharpoons & n_{10}^* \\
\beta_n^*/k^9 & & \beta_n^*/k^8 & & \beta_n^*/k^7 & & \beta_n^*/k & & \beta_n^* &
\end{array} \quad (10)$$

where state n_{10}^* is the only open state. Although Eq. (10) defines a Markov process, the dwell-time distribution in the closed state will closely follow a power-law distribution of the kind in Eq. (4) for times t in the range $1/\alpha_n^* \ll t \ll k^9/(k\alpha_n^* + \beta_n^*)$, for k not too large, due to the scaling behavior of this equation [37]. Each of the stages differs from the next only by a scaling factor, k ; such self-similarity imparts fractal behavior onto this simulated ion channel. Single-channel data from K^+ channels in cultured mouse hippocampal neurons yield $k=4$ [17]; for 11 states, this yields a closed-time distribution with smooth power-law behavior over roughly six decades. Closed-time distributions for this model, while analytically tractable, prove quite complicated. For convenience, we treat instead the case of an infinite chain of closed states, with the left-hand side of Eq. (10) extending without limit. With the help of renormalization theory we obtain

$$\begin{aligned}
E[T_O] &= 1/\beta_n^*, \\
E[T_C] &= 1/(\alpha_n^* - \beta_n^*).
\end{aligned} \quad (11)$$

Setting the respective forms for $E[T_O]$ and $E[T_C]$ in Eqs. (9) and (11) equal yields

$$\begin{aligned}
\beta_n^* &= 4\beta_n, \\
\alpha_n^* &= \frac{4(\alpha_n + \beta_n)^4 \beta_n}{(\alpha_n + \beta_n)^4 - \alpha_n^4}.
\end{aligned} \quad (12)$$

While this choice of α_n^* and β_n^* yields identical average dwell times to that of the classical (nonfractal) Hodgkin-Huxley model in the steady state, the existence of long memory in the closed-time distribution leads to changed properties of the Hodgkin-Huxley system. In particular, the fractal Hodgkin-Huxley model thus generated exhibited a significantly lower average firing rate than the Markov Hodgkin-Huxley system. To facilitate comparison with the Markov simulations, we adjusted the input current to match the average interspike intervals obtained in that case; the resulting values were 40 and 80 $\mu A/cm^2$, respectively, for the runs which matched the two nonfractal Hodgkin-Huxley runs listed earlier in average rate. These simulations were run for 103 873 and 100 559 spike events, respectively.

E. Data analysis

The action potentials by which neurons transmit information over macroscopic distances are comprised of a series of brief electrical spikes, the amplitude and energy of which are widely assumed not to be significant variables. Rather, it is generally accepted that the times of occurrences of the spikes carry the information. Randomness is involved, since ensembles of identical single-neuron experiments lead to dif-

fering sequences of nerve firings. A stochastic point process [38] is a mathematical construction which represents these firing events as random points on a line.

Figure 1 shows several representations that are useful in the analysis of point processes. Figure 1(a) demonstrates a sample function of a point process as a series of impulses occurring at specified times t_n . Since these impulses have vanishing width, they are most rigorously defined as the derivative of a well-defined counting process $N(t)$ [Fig. 1(b)], a monotonically increasing function of t , that augments by unity when a firing event occurs. Accordingly, the point process itself is properly written as $dN(t)$, since it is only strictly defined within the context of an integral.

The point process is completely described by the set of firing event times $\{t_n\}$, or equivalently by the set of inter-event intervals $\{\tau_n\}$. However, the sequence of counts depicted in Fig. 1(c) also contains much information about the process. Here the time axis is divided into equally spaced contiguous counting windows of duration T sec to produce a

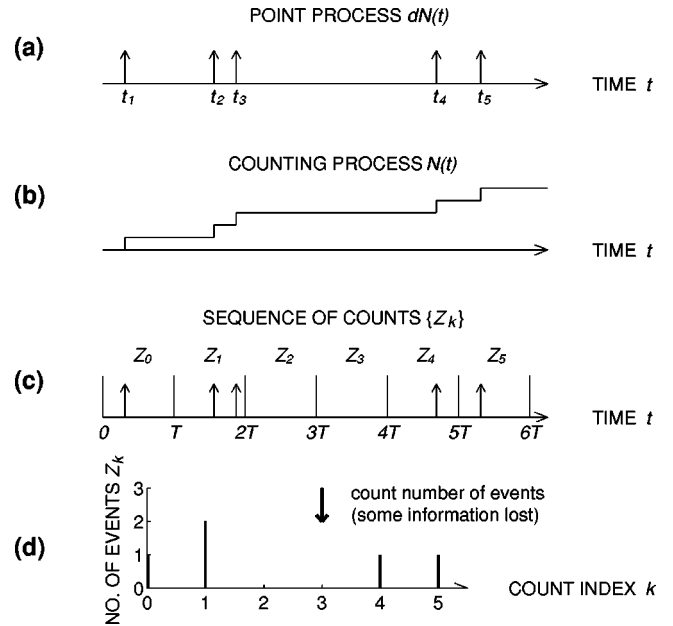


FIG. 1. Representations of a point process. (a) The events are represented by a sequence of idealized impulses, occurring at times t_n , and forming a stochastic point process $dN(t)$. For convenience of analysis, several alternative representations of the point process are used. (b) The counting process $N(t)$. At every spike occurrence the value of $N(t)$ augments by unity. (c) The sequence of counts $\{Z_k\}$, a discrete-time non-negative integer-valued stochastic process, is formed from the point process by recording the number of spikes in successive counting windows of length T . (d) The sequence of counts $\{Z_k\}$ can be conveniently described in terms of a count index k . Information is lost because the precise times of spike occurrences within each counting window are eliminated in this representation. Correlations in the discrete-time sequence $\{Z_k\}$ can be readily interpreted in terms of real time.

sequence of counts $\{Z_k\}$, where $Z_k = N[(k+1)T] - N[kT]$ denotes the number of firing events in the k th window. As illustrated in Fig. 1(d), this sequence forms a discrete-time random process of non-negative integers. In general, information is lost in forming the sequence of counts, although for a regular point process the amount lost can be made arbitrarily small by reducing the size of the counting window T . An attractive feature of this representation is that it preserves the correspondence between the discrete time axis of the counting process $\{Z_k\}$ and the absolute “real” time axis of the underlying point process. Within the process of counts $\{Z_k\}$, the elements Z_k and Z_{k+n} refer to the number of counts in windows separated by precisely $(n-1)T$ sec, so that correlation in the process $\{Z_k\}$ is readily associated with correlation in the underlying point process $dN(t)$.

The complete characterization of a stochastic process involves a description of all possible joint probabilities of the various firing events occurring in the process. Different statistics provide complementary views of the process; no single statistic can describe in general a stochastic process completely. For example, statistics that describe the relative occurrences of the interspike intervals (such as the interspike interval histogram, see Sec. II E 1) cannot distinguish between two point processes containing the same intervals but in a different order.

The point processes corresponding to neuronal firing patterns are not true fractals in time, since the associated generalized dimensions are not fractional [30,31,39]. However, the *rate* of firing is indeed a fractal, and turns out to be closely related to fractal Brownian motion. Thus neuronal firing behavior is well described by fractal-rate stochastic point processes [39], for which the Allan factor (Sec. II E 3) and the periodogram (Sec. II E 4) exhibit scaling. Such scaling leads naturally to power-law behavior [39], so that scaling of these statistics implies that the Fitzhugh-Nagumo and Hodgkin-Huxley simulations are well modeled by a process with a fractal rate, and therefore indeed have a fractal rate much as biological neurons do.

1. ISI histogram

The interspike-interval (ISI) histogram is simply the relative frequency of interspike-interval occurrence in the data set, ignoring all correlations among the intervals. The ISI histogram therefore cannot distinguish between processes with a fractal rate and those with a nonfractal rate. The only type of point process which is uniquely specified by the ISI histogram is the renewal point process family, in which the interspike intervals are independent and all drawn from the same distribution.

2. Rate function

Perhaps the simplest measure of neuronal activity is the estimate of the rate: the number of spikes registered per unit time [40]. In terms of the numbers of counts Z_k introduced in Sec. II E, the rate estimate $\hat{\lambda}_k$ of the k th window of duration T is given by $\hat{\lambda}_k = Z_k/T$. For a process with a fractal rate, the rate estimates exhibit fluctuations whose magnitude (e.g., the standard deviation) decreases more slowly, as the counting time used to compute the rate increases, than would be expected for processes with nonfractal rates.

3. Periodogram

The periodogram is an estimator of the power spectral density $S(f)$. Much as for continuous-time processes, the power spectral density computed for the neural spike events reveals how power is concentrated in various frequency bands. In general, the power spectral density varies with frequency, the sole exception being the homogeneous Poisson process, for which $S(f) = \lambda$ for all frequencies f . The homogeneous Poisson process corresponds to memoryless processes such as the registration of radioactive decay events, and provides an important benchmark in point-process theory just as the Gaussian does in the theory of continuous stochastic processes. Any deviation from λ in the value of $S(f)$ therefore indicates that the point process in question is not homogeneous Poisson in nature. In the case of a *fractal* rate, the power spectral density decreases as a power-law function of frequency over a broad range of frequencies, so that $S(f) \sim f^{-b_s}$ for some power-law exponent b_s .

We employ the periodogram of the sequence of counts $\{Z_k\}$, rather than from the point process itself [41]. This method introduces a bias at higher frequencies, since the fine time resolution information is lost as a result of the nonzero size of the count windows. However, the component of a process which imparts a fractal quality to its rate principally involves lower frequencies where this bias is negligible, and thus the difference between the two methods does not significantly affect our results. Since employing the sequence of counts permits the use of vastly more efficient fast Fourier transform methods, impossible for a periodogram based on the point process itself, we employ this technique.

4. Allan factor

Another measure of correlation over different time scales is provided by the Allan factor, a relative variance based on a particular wavelet transform [42]. The Allan factor $A(T)$ is the Allan variance of the number of spikes in a specified counting time T divided by twice the mean number of spikes in that counting time. The Allan variance is defined in terms of the variability of successive counts [43,44]. In terms of the sequence $\{Z_k\}$ illustrated in Fig. 1(c), the Allan factor becomes

$$A(T) \equiv \frac{E[(Z_{k+1} - Z_k)^2]}{2E[Z_k]}. \quad (13)$$

In general the Allan factor also varies as a function of its argument, with the sole exception again being the homogeneous Poisson process, for which $A(T) = 1$ for all counting times T . For any point process, the Allan factor assumes a value of unity for counting times T less than half the smallest interspike interval. The Allan factor of a process with a fractal rate increases as a power-law function of the counting time over a broad range of counting times, so that $A(T) \sim T^{b_A}$ for some power-law exponent b_A , where $0 < b_A \leq 3$.

The Allan factor and the power spectral density are related by the integral equation

$$A(T) = \frac{2}{\pi^2 \lambda T} \int_{-\infty}^{\infty} S(f) \sin^4(\pi f T) f^{-2} df. \quad (14)$$

TABLE I. Statistics for Markov- and fractal-channel Fitzhugh-Nagumo simulations with different input currents, and for the auditory-nerve recording.

	Markov		Fractal		Auditory Neuron
	Run 1	Run 2	Run 1	Run 2	
Duration (sec)	219999	220000	86554700	80626300	1799.18
Number of spikes	294827	294884	166801	213696	127500
Mean interspike interval (sec)	0.746198	0.746056	518.91	377.294	0.0141112

In particular, for processes with fractal rates for which the power-law behavior of the Allan factor extends to arbitrarily large frequencies, and for which $0 < b_A < 3$, we have the theoretical result $b_A = b_S$. In practice, the finite length of any data set will introduce significant bias and variance into estimates of b_S , and some variance into estimates of b_A , so that exact agreement will not be obtained [39].

III. RESULTS

A. Fitzhugh-Nagumo

Rate estimates of the raw simulation results for the fractal-channel Fitzhugh-Nagumo model (not shown) exhibited apparent nonstationarity at the beginning. This is likely due to memory of the initial condition stored in the states of the channels, although equilibrium distributions were employed in the initialization of the simulations (suggesting that this system typically does not remain near equilibrium). To ensure stationarity, the first 25% of the spikes were discarded. The Markov-channel Fitzhugh-Nagumo simulations showed no such nonstationarity, and therefore no spikes were discarded from these simulations.

The mean interspike intervals of the fractal-channel Fitzhugh-Nagumo simulations differed significantly from each other, and differed greatly from those of the Markov-channel Fitzhugh-Nagumo simulations, as shown in Table I. To facilitate comparisons among the different simulations and the representative neural recording, all data sets were normalized by dividing the interspike intervals by their respective means before subsequent data analysis. The resulting normalized results have their average interspike intervals all set to the same value (unity), but all other characteristics of the spike trains remain unchanged by the normalization procedure. In particular, this procedure is irrelevant to the presence or absence of fractal behavior.

1. ISI histogram

For the discrete-channel Fitzhugh-Nagumo models, the Markov- and fractal-channel simulations exhibit substantially different interspike-interval distributions from each other and from the representative neural recording, even when normalized by their respective means (see Fig. 2). The Markov-channel simulations generate much narrower and more repeatable distributions than their fractal-channel counterparts. Evidently, fractal ion-channel behavior in a Fitzhugh-Nagumo model leads to long-term fluctuations which do not average out over the course of an interspike interval, and which lead to a broadening of the interval distribution. The neural recording yields an ISI histogram resembling that of the fractal-channel Fitzhugh-Nagumo

model, although slightly narrower. The excess of interspike intervals near the smallest intervals shown in this neuron often occurs in auditory-nerve recordings [45].

2. Rate function

Fractal ion channels in Fitzhugh-Nagumo simulations yield firing rate estimates which exhibit fluctuations over long time scales, several times the 5000 sec windows used to construct the rate estimates in this example (see Fig. 3). Such fluctuations appear not to be artifacts of nonstationarities, since no apparent trends can be observed in the data (after the first 25% of the intervals have been removed, as specified above). The auditory-nerve recording exhibits similar, although somewhat smaller, fluctuations. The Markov-channel simulations, in contrast, exhibit almost undetectable fluctuations as is typical for nonfractal point processes averaged over 5000 intervals.

3. Allan factor

Simulations employing Markov ion channels yield Allan factor plots which decrease to small values for larger counting times, indicating that the firing is a comparably regular

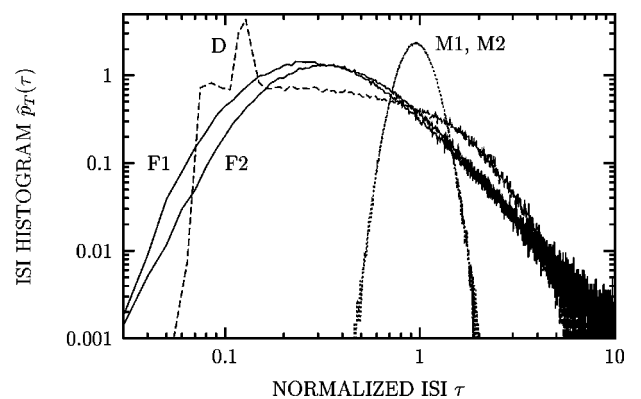


FIG. 2. Doubly logarithmic plots of the interspike-interval (ISI) histogram $\widehat{p}_T(\tau)$ vs normalized interspike interval τ , for Fitzhugh-Nagumo simulations and the auditory-nerve recording. Solid lines indicate histograms constructed from fractal-channel simulations (labeled ‘‘F1’’ and ‘‘F2’’ for runs 1 and 2, respectively); dotted curves derive from Markov-channel simulations (labeled ‘‘M1’’ and ‘‘M2’’ for runs 1 and 2, respectively); and the dashed curve is from the auditory-nerve data (labeled ‘‘D’’). As with the mean interspike intervals, the forms of the ISI histogram plots for the fractal-channel simulations differ from each other, and differ greatly from those of the Markov-channel simulations. The Markov-channel simulations yield ISI histogram plots in close agreement with each other. The ISI histogram of the neural recording resembles that of the fractal-channel Fitzhugh-Nagumo

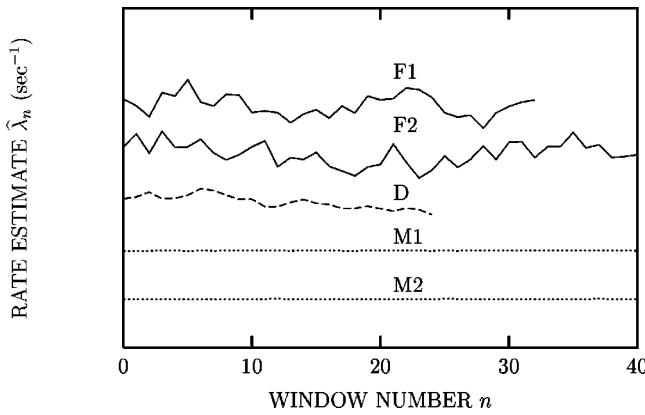


FIG. 3. Doubly linear plots of estimates of the normalized rate $\hat{\lambda}_n$ vs window number n , for Fitzhugh-Nagumo simulations and the auditory-nerve recording. Rates are calculated over a counting window of 5000 normalized time units. Solid lines indicate rate functions constructed from fractal-channel simulations (labeled “F1” and “F2” for runs 1 and 2, respectively); dotted curves derive from Markov-channel simulations (labeled “M1” and “M2” for runs 1 and 2, respectively); and the dashed curve is from the auditory-nerve data (labeled “D”). All rate functions have unity means (by construction) but are vertically displaced for display purposes; the vertical extent of the plot corresponds to a rate difference of six. The rate functions for the fractal-channel simulations and auditory-nerve recording exhibit significant fluctuations (upper three curves); the Markov-channel simulations, in contrast, appear almost perfectly flat at these window sizes (lower two curves).

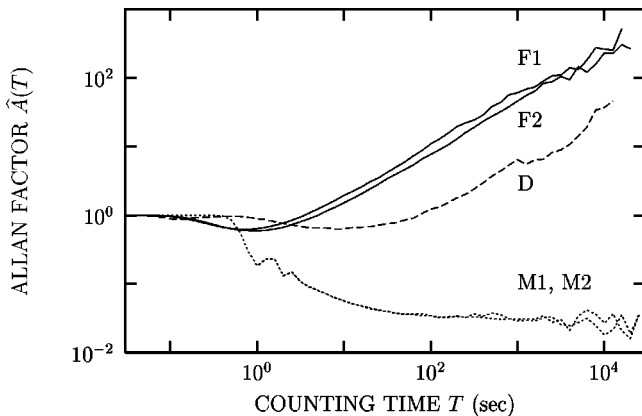


FIG. 4. Doubly logarithmic plots of estimates of the Allan factor $\hat{A}(T)$ vs counting time T , for Fitzhugh-Nagumo simulations and the auditory-nerve recording. Solid lines indicate estimated Allan factors constructed from fractal-channel simulations (labeled “F1” and “F2” for runs 1 and 2, respectively); dotted curves derive from Markov-channel simulations (labeled “M1” and “M2” for runs 1 and 2, respectively); and the dashed curve is from the auditory-nerve data (labeled “D”). Markov-channel simulations yield plots which decrease well below unity, indicating a firing pattern which is quite regular. Allan factor plots of fractal-channel simulations exhibit a power-law increase with counting time, indicative of fractal firing behavior. Estimated slopes are 0.68 and 0.69 for runs 1 and 2, respectively. The auditory-nerve recording yields similar behavior, with an estimated slope of 0.71.

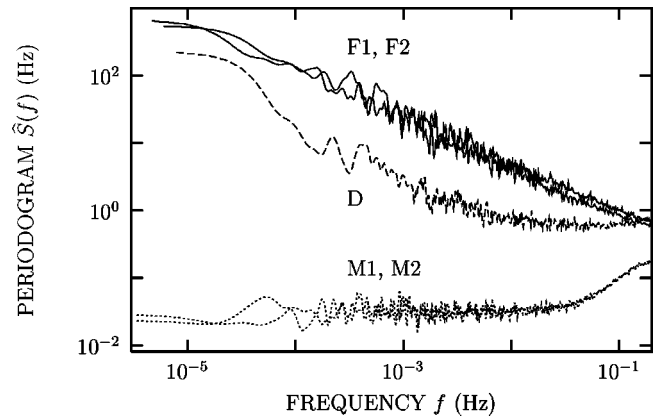


FIG. 5. Doubly logarithmic plots of the periodogram $\hat{S}(f)$, an estimate of the power spectral density, vs frequency f , for Fitzhugh-Nagumo simulations and the auditory-nerve recording. Solid lines indicate periodograms constructed from fractal-channel simulations (labeled “F1” and “F2” for runs 1 and 2, respectively); dotted curves derive from Markov-channel simulations (labeled “M1” and “M2” for runs 1 and 2, respectively); and the dashed curve is from the auditory-nerve data (labeled “D”). Markov-channel simulations yield periodograms which remain at small values, indicating a firing pattern which is quite regular. Periodograms of fractal-channel simulations and of the auditory neuron data, on the other hand, exhibit a power-law decrease with frequency, indicative of fractal firing behavior. Estimated slopes are 0.63 and 0.64 for runs 1 and 2, respectively, for the fractal-channel simulations, and 0.54 for the auditory-nerve recording.

process (see Fig. 4). This is consistent with the narrow ISI histogram shown in Fig. 2 and the absence of any fractal-rate behavior. Introducing fractal ion channels, on the other hand, results in Allan factor plots which increase as power-law functions of the counting time (straight lines on a doubly logarithmic plot), with an estimated slope of 0.69 ± 0.005 [39]. The auditory-nerve recording also exhibits a power-law form, with an estimated slope of 0.71, but with a smaller magnitude at larger counting times consistent with the smaller fluctuations in the rate function shown in Fig. 3. This is a hallmark of fractal-rate firing activity.

4. Periodogram

The periodogram yields results in substantial accord with those of the Allan factor (see Fig. 5). For the Markov-channel simulations, the resulting periodograms remain below unity for smaller frequencies, again consistent with an orderly sequence of firings. For the fractal-channel simulations, the periodograms decrease as power-law functions of frequency, with estimated slopes of 0.63 and 0.64 for runs 1 and 2, respectively; the auditory-nerve recording yields an estimated slope of 0.54 [39]. This measure also reveals fractal activity of somewhat reduced strength compared to the simulations, in accord with Figs. 3 and 4. Power-law exponents computed from the periodogram exhibit bias and often more variance than those from the Allan factor, so these exponent values are in reasonable agreement for the number of spikes available [39].

5. Fitzhugh-Nagumo summary

Modifying the Fitzhugh-Nagumo equations to include Markov (random) channels indeed introduces randomness to

TABLE II. Statistics for Markov- and fractal-channel Hodgkin-Huxley simulations with different input currents, and for the auditory-nerve recording. As intended, both simulations labeled ‘‘Run 1’’ have mean interspike intervals in rough agreement, as do those labeled ‘‘Run 2.’’

	Markov		Fractal		Auditory Neuron
	Run 1	Run 2	Run 1	Run 2	
Input current ($\mu\text{A}/\text{cm}^2$)	-4	0	40	80	
Duration (sec)	14502.8	2999.97	12280.8	2999.99	1799.18
Number of spikes	87905	117027	103873	100559	127500
Mean interspike interval (sec)	0.164983	0.0256348	0.118229	0.0298331	0.0141112

the subsequent firing pattern. Being Markov, the channels have only short-term memory, so that the sequence of firing events behaves as a renewal point process. Employing channels which have fractal open- and closed-time distributions, however, leads to dramatically different behavior. The memory thus introduced in the channel states increases the average interspike interval, since a much longer time is required for the state to change and permit a firing event. The channel memory also leads to a broader interspike-interval distribution (even after normalization), since the channel states will not average out during the course of a single interval. Finally, the resulting firing process has a fractal rate, as evidenced by both second-order statistical measures employed (Allan factor and periodogram). Thus, for the Fitzhugh-Nagumo model with individual ion channels, fractal channel behavior indeed generates fractal firing behavior. Such behavior also resembles natural fractal activity occurring in the representative biological neuron shown, although the simulations exhibit a stronger fractal component than that of the biological data. Perhaps some nonfractal component, such as Markov behavior, would prove useful in generating results in close agreement with the biological data.

B. Hodgkin-Huxley

The mean interspike intervals of both the Markov- and fractal-channel Hodgkin-Huxley simulations varied with the input current, as expected (see Table II). To facilitate comparisons among the different simulations, all were normalized by dividing the interspike intervals by their respective mean before subsequent data analysis, as was done for the Fitzhugh-Nagumo simulations.

1. ISI histogram

In contrast to the results for the Fitzhugh-Nagumo model, for the discrete-channel Hodgkin-Huxley models the Markov- and fractal-channel simulations exhibit interspike-interval distributions which resemble each other and that of the auditory neuron; both the means and the overall shapes are similar (see Fig. 6; auditory-nerve data are replotted from Fig. 2 for comparison). For the more negative input currents, the results of the Markov- and fractal-channel simulations follow essentially the same form. Run 2, with a higher rate, does show some broadening of the interval distribution for the fractal-channel case. This likely stems from long-term fluctuations which do not average out over the course of an interspike interval, as also observed in the Fitzhugh-Nagumo

models. For the Hodgkin-Huxley model, then, the addition of fractal ion-channel behavior also changes the interval distribution, but not substantially. As previously mentioned, auditory-nerve recordings often exhibit an excess of interspike intervals near the smallest intervals [45].

2. Rate function

As with the Fitzhugh-Nagumo model, fractal ion channels in Hodgkin-Huxley simulations yield firing rate estimates which exhibit fluctuations over long time scales, several times the 2500 sec windows used to construct the rate estimates in this example (see Fig. 7). Again, such fluctuations appear not to be artifacts of nonstationarities, since no apparent trends can be observed in the data. These rate estimates also resemble that of the auditory-nerve recording, replotted from Fig. 3. The Markov-channel simulations, in contrast, exhibit much smaller fluctuations as is typical for nonfractal point processes averaged over 2500 intervals. In addition, simulations that are run at lower currents (run 1) show somewhat larger fluctuations than those at higher currents (run 2), as expected.

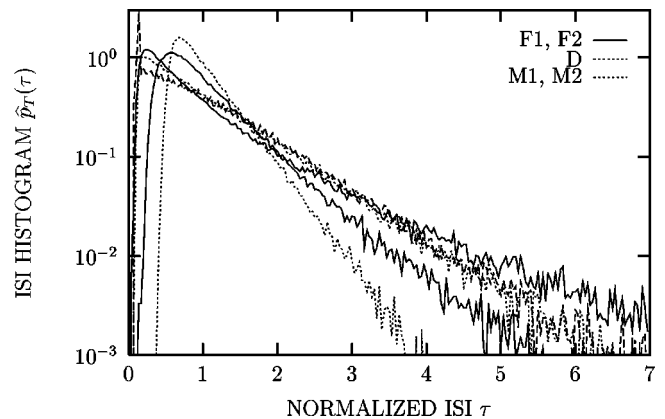


FIG. 6. Semilogarithmic plots of the interspike-interval (ISI) histogram $\hat{p}_T(\tau)$ vs normalized interspike interval τ , for Hodgkin-Huxley simulations and the auditory-nerve recording. Solid lines indicate histograms constructed from fractal-channel simulations (labeled ‘‘F1’’ and ‘‘F2’’ for runs 1 and 2, respectively); dotted curves derive from Markov-channel simulations (labeled ‘‘M1’’ and ‘‘M2’’ for runs 1 and 2, respectively); and the dashed curve is from the auditory-nerve data (labeled ‘‘D’’). All five plots agree in overall shape and mean. For run 1, the results of the Markov- and fractal-channel simulations follow essentially the same form, while the Markov-channel simulation yields a slightly more peaked histogram than the fractal-channel version for run 2.

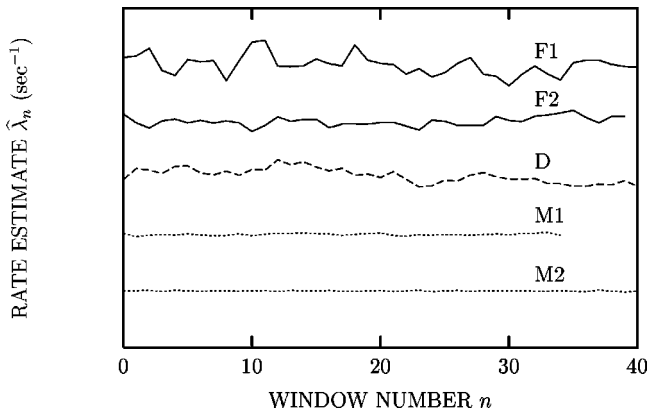


FIG. 7. Doubly linear plots of estimates of the normalized rate $\hat{\lambda}_n$ vs window number n , for Hodgkin-Huxley simulations and the auditory-nerve recording. Rates are calculated over a counting window of 2500 normalized time units. Solid lines indicate rate functions constructed from fractal-channel simulations (labeled “F1” and “F2” for runs 1 and 2, respectively); dotted curves derive from Markov-channel simulations (labeled “M1” and “M2” for runs 1 and 2, respectively); and the dashed curve is from the auditory-nerve data (labeled “D”). All rate functions have unity means (by construction) but are vertically displaced for display purposes; the vertical extent of the plot corresponds to a rate difference of six. The rate functions for the fractal-channel simulations and auditory nerve recording exhibit significant fluctuations (upper three curves); the Markov-channel simulations, in contrast, appear much more flat at these window sizes (lower two curves). For both types of channels, run 1 exhibits somewhat more fluctuations than run 2.

3. Allan factor

Simulations employing Markov ion channels yield Allan factor plots which decrease for larger counting times, indicating that the firing is a comparably regular process (see Fig. 8). Introducing fractal ion channels, on the other hand, results in Allan factor plots which increase as power-law function of the counting time (straight lines on a doubly logarithmic plot), with estimated slopes of 0.82 and 0.68 for runs 1 and 2, respectively [39]. These curves resemble the Allan factor of the auditory-nerve recording, replotted from Fig. 4, which has an estimated slope of 0.73. Thus the Hodgkin-Huxley simulations with fractal channels exhibit fractal-rate firing activity as do the corresponding Fitzhugh-Nagumo simulations.

4. Periodogram

As with the Fitzhugh-Nagumo simulations, the periodogram (see Fig. 9) yields results in substantial accord with those of the Allan factor. For the Markov-channel simulations, the resulting periodograms remain below unity for smaller frequencies, again consistent with an orderly sequence of firings. For the fractal-channel simulations, the periodograms decrease as power-law functions of frequency, with estimated slopes of 0.47 and 0.49 for runs 1 and 2, respectively; the auditory-nerve recording yields an estimated slope of 0.54 [39]. As with the Fitzhugh-Nagumo simulations, these values differ from those obtained from the

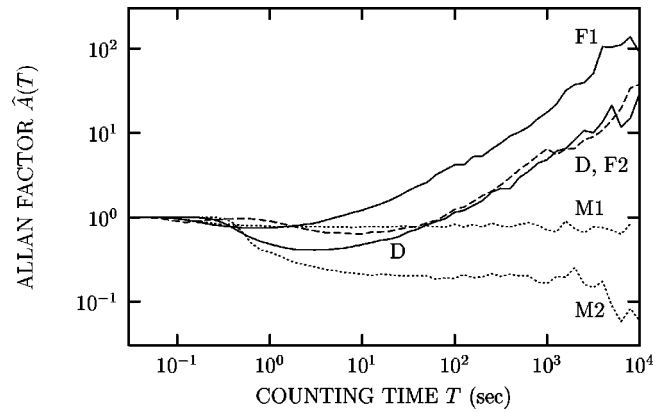


FIG. 8. Doubly logarithmic plots of estimates of the Allan factor $\hat{A}(T)$ vs counting time T , for Hodgkin-Huxley simulations and the auditory-nerve recording. Solid lines indicate estimated Allan factors constructed from fractal-channel simulations (labeled “F1” and “F2” for runs 1 and 2, respectively); dotted curves derive from Markov-channel simulations (labeled “M1” and “M2” for runs 1 and 2, respectively); and the dashed curve is from the auditory-nerve data (labeled “D”). Markov-channel simulations yield plots which decrease below unity, indicating a firing pattern which is fairly regular. Allan factor plots of fractal-channel simulations, on the other hand, exhibit a power-law increase with counting time, indicative of fractal firing behavior. Estimated slopes are 0.82 and 0.68 for runs 1 and 2, respectively. The auditory-nerve recording yields similar behavior, with an estimated slope of 0.71.

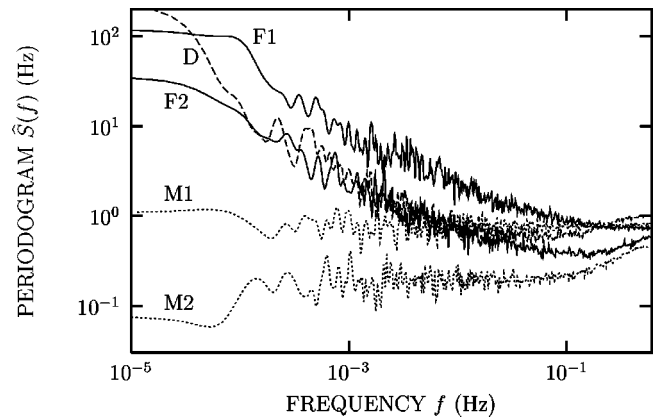


FIG. 9. Doubly logarithmic plots of the periodogram $\hat{S}(f)$, an estimate of the power spectral density, vs frequency f , for Hodgkin-Huxley simulations and the auditory-nerve recording. Solid lines indicate periodograms constructed from fractal-channel simulations (labeled “F1” and “F2” for runs 1 and 2, respectively); dotted curves derive from Markov-channel simulations (labeled “M1” and “M2” for runs 1 and 2, respectively); and the dashed curve is from the auditory-nerve data (labeled “D”). Markov-channel simulations yield periodograms which remain at small values, indicating a firing pattern which is quite regular. Periodograms of fractal-channel simulations, on the other hand, exhibit a power-law decrease with frequency, indicative of fractal firing behavior. Estimated slopes are 0.47 and 0.49 for runs 1 and 2, respectively, for the fractal-channel simulations, and 0.54 for the auditory-nerve recording.

Allan factor, likely due to the inferior performance of periodogram-based exponent estimates [39].

5. Hodgkin-Huxley summary

As with the Fitzhugh-Nagumo simulations, modifying the Hodgkin-Huxley equations to include channels with fractal behavior in time changes the long-term properties of the resulting simulated spike trains. A fractal rate again results, as evidenced by both second-order statistical measures employed (Allan factor and periodogram). In contrast to the Fitzhugh-Nagumo model, however, the normalized interspike interval histograms do not differ significantly from their Markov-channel counterparts, with the average interspike intervals set to the same values by adjusting the input current. Just as for the Fitzhugh-Nagumo model, for the Hodgkin-Huxley model fractal channel behavior indeed generates fractal firing behavior. In addition, the results more closely resemble those of neuronal data.

IV. DISCUSSION

In this paper we have studied the effects of imparting fractal behavior to the ion channels using two different methods: a direct modification of the dwell time distribution for the Fitzhugh-Nagumo model, and a self-similar quasifractal chain of states for the Hodgkin-Huxley model. In both cases, the result is the same: fractal ion channel behavior leads to fractal firing behavior. This causal relationship is emphasized by the fact that removal of fractal correlations in ion channel statistics obliterates fractal firing patterns. It is important to note that this effect does not depend on whether the fractal behavior in ion channels arises from intrinsic properties of the ion channels themselves, or by other mechanisms.

A. The relationship between ion channel and spiking characteristics proves difficult to quantify

Although we provide strong evidence here that fractal or quasifractal dwell times for voltage-gated ion channels can generate fractal spiking patterns, two factors make it very difficult, if not impossible, to make quantitative inferences about the characteristics of ion channels (fractal or otherwise) from spike train data, and vice versa. First, both the Fitzhugh-Nagumo and Hodgkin-Huxley models generate spikes that are stereotypical in form. Detailed information about the state of the model over time scales much shorter than the time between spikes is inevitably lost in the process of spike generation. This loss of information renders precise estimation of the parameters of the ion channels from the spike train alone impossible. Other forms of fractal ion channels, or even other models, therefore might be able to generate a sequence of spikes with a fractal rate. Second, while the fractal Fitzhugh-Nagumo and Hodgkin-Huxley models employed in this paper have well-defined fractal exponents in the steady state, channel parameters change with membrane voltage. During the time between one spike and the next the membrane voltage assumes a wide range of values, which in turn generates a time-varying power-law exponent for the ion channels. The effects of voltage-dependent ion

channel properties have been characterized for simple cases [46–48], but not for the case we study here, which includes power-law exponents and the additional complexity that channel states perturb the input voltage signal. The resulting interaction produces a spike train that has a fractal rate, but the associated power-law exponent b will depend on the details of the ion channel behavior as a function of voltage, the time since the channel last changed state, and the details of how ion channel state affects voltage.

B. Modeling fractal ion channels proves challenging

The modeling method taken here, which depends on closed-time probability density functions that decay as power laws, presents difficulties. Theoretical difficulties arise from the fact that a true power-law probability density function would have a divergent integral. We solved this problem by employing an explicit cutoff [t_0 in Eq. (4)] for the fractal Fitzhugh-Nagumo simulations, and a self-similar Markov chain for the fractal Hodgkin-Huxley simulations. Although the two methodologies differ, over the designed range of time scales they yield similar smooth fractal behavior.

Practical difficulties in running simulations arise from the basic nature of fractal ion channels, which necessarily implies that a significant fraction of the channels must remain unchanged in their conductance state over long time scales. Nevertheless, for the model to successfully fire, a significant number of ion channels must indeed change state, so that the simulation voltage (or fast variable) can reach threshold. These two requirements — that significant numbers of channels not change state (to preserve memory), and that significant numbers do change (to enable firing) — place severe constraints on our ability to simulate spike trains of adequate length in a reasonable amount of time. For example, in our treatment of the Hodgkin-Huxley model, in order to have “settling” times of practical duration, we were forced to limit the number of states of our modified K^+ channel to 11 — a number that was small enough to perturb upward the steady-state probability of opening. (Recall that our pseudo-fractal formulation only matched the steady-state probability of opening in the limit of an infinite number of states.) This perturbation, in turn, reduced the spontaneous firing rate of the model, making it more time-consuming to collect the large number of interspike intervals needed for our analyses. This issue would be even more problematic with fractal modifications of typical mammalian K^+ channels, which are more likely to be closed at rest than Hodgkin-Huxley channels [49] and thus more perturbed by the finite-state fractal channel approximation. This difficulty could perhaps be overcome by including two populations of K^+ channels in the model: a low-threshold population with fractal characteristics to give long-term memory, and high-threshold population with Markov characteristics to repolarize action potentials.

ACKNOWLEDGMENTS

S.B.L. and J.A.W. acknowledge the support of The Whitaker Foundation, and L.S.L. acknowledges the support of NIH under Grant No. NEI06234.

- [1] A. L. Hodgkin and A. F. Huxley, *J. Physiol. (London)* **117**, 500 (1952).
- [2] B. Hille, *Ionic Channels of Excitable Membranes*, 2nd ed. (Sinauer Associates, Sunderland, MA, 1992).
- [3] B. Sakmann and E. Neher, *Single-Channel Recording*, 2nd ed. (Plenum, New York, 1995).
- [4] R. H. Austin *et al.*, *Biochemistry* **14**, 5355 (1975).
- [5] M. L. Saviotti and W. C. Galley, *Proc. Natl. Acad. Sci. USA* **71**, 4154 (1974).
- [6] F. R. N. Gurd and T. M. Rothgeb, *Adv. Protein Chem.* **33**, 73 (1979).
- [7] D. Ringe and G. A. Petski, *Prog. Biophys. Mol. Biol.* **45**, 197 (1984).
- [8] G. R. Welch, *The Fluctuating Enzyme* (John Wiley and Sons, New York, 1986).
- [9] J. R. Alcalá, E. Gratton, and F. G. Prendergast, *Biophys. J.* **51**, 925 (1987).
- [10] S. W. Englander *et al.*, *Science* **256**, 1684 (1992).
- [11] J. A. McCammon and S. C. Harvey, *Dynamics of Proteins and Nucleic Acids* (Cambridge University Press, New York, 1987).
- [12] M. Karplus and G. A. Petsko, *Nature (London)* **347**, 631 (1990).
- [13] A. Fuliński *et al.*, *Phys. Rev. E* **58**, 919 (1998).
- [14] B. B. Mandelbrot, *The Fractal Geometry of Nature*, 2nd ed. (W. H. Freeman, New York, 1983).
- [15] J. B. Bassingthwaite, L. S. Liebovitch, and B. J. West, *Fractal Physiology* (Oxford, New York, 1994).
- [16] L. S. Liebovitch, J. Fischbarg, and J. P. Koniarek, *Math. Biosci.* **84**, 37 (1987).
- [17] L. S. Liebovitch and J. M. Sullivan, *Biophys. J.* **52**, 979 (1987).
- [18] A. Toib, V. Lyakhov, and S. Marom, *J. Neurosci.* **18**, 1893 (1998).
- [19] N. L. Powers, R. J. Salvi, and S. S. Saunders, in *Abstracts of the XIV Midwinter Research Meeting, Association for Research in Otolaryngology*, edited by D. J. Lim (Association for Research in Otolaryngology, Des Moines, IA, 1991), p. 129, abstract 411.
- [20] N. L. Powers and R. J. Salvi, in *Abstracts of the XV Midwinter Research Meeting, Association for Research in Otolaryngology*, edited by D. J. Lim (Association for Research in Otolaryngology, Des Moines, IA, 1992), p. 101, abstract 292.
- [21] O. E. Kelly, D. H. Johnson, B. Delgutte, and P. Cariani, *J. Acoust. Soc. Am.* **99**, 2210 (1996).
- [22] M. C. Teich *et al.*, *J. Opt. Soc. Am. A* **14**, 529 (1997).
- [23] R. G. Turcott, P. D. R. Barker, and M. C. Teich, *J. Stat. Comput. Simul.* **52**, 253 (1995).
- [24] M. E. Wise, in *Statistical Distributions in Scientific Work*, edited by C. E. A. Taillie, G. P. Patil, and B. A. Baldessari (D. Reidel, Boston, 1981), Vol. 6, pp. 211–231.
- [25] F. Grüneis *et al.*, *Biol. Cybern.* **68**, 193 (1993).
- [26] S. B. Lowen and M. C. Teich, *J. Acoust. Soc. Am.* **99**, 3585 (1996).
- [27] Data collected at the Eaton-Peabody Laboratory and provided by Don Johnson.
- [28] M. C. Teich, *IEEE Trans. Biomed. Eng.* **36**, 150 (1989).
- [29] M. C. Teich, R. G. Turcott, and S. B. Lowen, in *The Mechanics and Biophysics of Hearing*, edited by P. Dallos *et al.*, *Lecture Notes in Biomathematics* Vol. 87 (Springer-Verlag, New York, 1990), pp. 354–361.
- [30] S. B. Lowen, S. S. Cash, M.-m. Poo, and M. C. Teich, *J. Neurosci.* **17**, 5666 (1997).
- [31] S. B. Lowen, S. S. Cash, M.-m. Poo, and M. C. Teich, in *Computational Neuroscience: Trends in Research 1997*, edited by J. M. Bower (Plenum Press, New York, 1997).
- [32] A. S. French and L. L. Stockbridge, *Can. J. Physiol. Pharmacol.* **66**, 967 (1988).
- [33] S. B. Lowen and M. C. Teich, *Fractals* **3**, 183 (1995).
- [34] C. C. Chow and J. A. White, *Biophys. J.* **71**, 3013 (1996).
- [35] D. T. Gillespie, *J. Phys. Chem.* **81**, 2340 (1977).
- [36] E. Skaugen and L. Walløe, *Acta Physiol. Scand.* **107**, 343 (1979).
- [37] L. S. Liebovitch, *Math. Biosci.* **93**, 97 (1989).
- [38] D. R. Cox and V. Isham, *Point Processes* (Chapman and Hall, London, 1980).
- [39] S. Thurner *et al.*, *Fractals* **5**, 565 (1997).
- [40] M. C. Teich, in *Single Neuron Computation*, edited by T. McKenna, J. Davis, and S. Zornetzer (Academic Press, Boston, 1992), pp. 589–625.
- [41] K. Matsuo, B. E. A. Saleh, and M. C. Teich, *J. Math. Phys.* **23**, 2353 (1982).
- [42] M. C. Teich, C. Heneghan, S. B. Lowen, and R. G. Turcott, in *Wavelets in Medicine and Biology*, edited by A. Aldroubi and M. Unser (CRC Press, Boca Raton, FL, 1996), Chap. 14, pp. 383–412.
- [43] D. W. Allan, *Proc. IEEE* **54**, 221 (1966).
- [44] J. A. Barnes and D. W. Allan, *Proc. IEEE* **54**, 176 (1966).
- [45] R. P. Gaumond, Ph.D. thesis, Washington University, St. Louis, MO, 1980.
- [46] S. M. Bezrukov and I. Vodyanoy, *Nature (London)* **385**, 319 (1997).
- [47] S. M. Bezrukov and I. Vodyanoy, *Biophys. J.* **73**, 2456 (1997).
- [48] S. M. Bezrukov, *Phys. Lett. A* **248**, 29 (1998).
- [49] B. Rudy, *Neuroscience (Oxford)* **25**, 729 (1988).